Research Article | Vol. 8, No. 3 | 1 Mar 2018 | OPTICAL MATERIALS EXPRESS 622
Optical Materials EXPRESS

Spectroscopic OCT: towards an effective tool for distinguishing authentic and artificial Chinese freshwater pearls

YANG ZHOU,[1,2] YANG ZHAO,[1] SANGHOON KIM,[1] AND ADAM WAX[1,*]

[1]*Department of Biomedical Engineering, Duke University, Durham, NC 27708, USA*
[2]*School of Information and Electronic Engineering, Zhejiang University of Science and Technology, Zhejiang 310023, China*
a.wax@duke.edu

Abstract: Distinguishing authentic and artificial Chinese freshwater pearls involves various tools and techniques, based primarily on visual inspection and spectroscopy. These methods are highly variable and thus not statistically reliable. This study investigates the capacity of spectroscopic optical coherence tomography (S-OCT) to classify authentic and artificial pearls in the NIR spectral range. The major advantage of S-OCT is that it allows spectroscopic measurements from within pearls, unlike traditional methods such as diffuse reflectance spectroscopy that primarily probe the surface. S-OCT spectral data was analyzed using principal component analysis (PCA) and partial least-squares discriminant analysis (PLSDA) to classify pearls. The implemented models successfully predicted pearl type and met performance metrics. The results show that S-OCT models could be used for more objective discrimination of authentic versus artificial pearls.

OCIS codes: (110.4500) Optical coherence tomography: (300.6170) Spectra.

References and links

1. D. Fiske and J. Shepherd, "Continuity and change in Chinese freshwater pearl culture," Gems & Gemology **43**(2), 138–145 (2007).
2. L. Kiefert, H. A. Haenni, and J.-P. Chalain, "Identification of gemstone treatments with Raman spectroscopy," Proc. SPIE **4098**, 241–251 (2000).
3. A. Aponick, E. Marchozzi, C. R. Johnston, and C. T. Wigal, "Determining the authenticity of gemstones using Raman spectroscopy," J. Chem. Educ. **75**(4), 465–466 (1998).
4. D. Bersani and P. P. Lottici, "Applications of Raman spectroscopy to gemology," Anal. Bioanal. Chem. **397**(7), 2631–2646 (2010).
5. B. Schrader, H. Schulz, G. N. Andreev, H. H. Klump, and J. Sawatzki, "Non-destructive NIR-FT-Raman spectroscopy of plant and animal tissues, of food and works of art," Talanta **53**(1), 35–45 (2000).
6. S. Karampelas, "Overview of pearl testing; classic methods and new developments," in *5th European Gemmological Symposium* (NEL & GGN Leiden, 2013), The Netherlands, pp 10–13.
7. S. Agatonovic-Kustrin and D. W. Morton, "The use of UV-visible reflectance spectroscopy as an objective tool to evaluate pearl quality," Mar. Drugs **10**(12), 1459–1475 (2012).
8. K. Nagai, "A history of the cultured pearl industry," Zool. Sci. **30**(10), 783–793 (2013).
9. M. S. Krzemnicki, S. D. Friess, P. Chalus, H. A. Hanni, and S. Karampelas, "X-Ray Computed Microtomography: Distinguishing Natural Pearls from Beaded and Non-Beaded Cultured Pearls," Gems & Gemology **46**(2), 128–134 (2010).
10. J. Rosc, V. M. F. Hammer, and R. Brunner, "X-ray computed tomography for fast and non-destructive multiple pearl inspection," Case Studies in Nondestructive Testing and Evaluation **6**, 32–37 (2016).
11. M. Loesdau, S. Chabrier, and A. Gabillon, "Computer vision based nacre thickness measurement of Tahitian pearls," In Thirteenth International Conference on Quality Control by Artificial Vision (International Society for Optics and Photonics, 2017), Vol. 10338.
12. M. J. Ju, S. J. Lee, Y. Kim, J. G. Shin, H. Y. Kim, Y. Lim, Y. Yasuno, and B. H. Lee, "Multimodal analysis of pearls and pearl treatments by using optical coherence tomography and fluorescence spectroscopy," Opt. Express **19**(7), 6420–6432 (2011).
13. E. A. Swanson and J. G. Fujimoto, "The ecosystem that powered the translation of OCT from fundamental research to clinical and commercial impact," Biomed. Opt. Express **8**(3), 1638–1664 (2017).
14. M. J. Ju, S. J. Lee, E. J. Min, Y. Kim, H. Y. Kim, and B. H. Lee, "Evaluating and identifying pearls and their nuclei by using optical coherence tomography," Opt. Express **18**(13), 13468–13477 (2010).

#314582 https://doi.org/10.1364/OME.8.000622
Journal © 2018 Received 1 Dec 2017; revised 3 Feb 2018; accepted 3 Feb 2018; published 13 Feb 2018

Optical Materials EXPRESS

15. Y. Zhou, T. Liu, Y. Shi, Z. Chen, J. Mao, and W. Zhou, "Automated internal classification of beadless Chinese Zhuji fleshwater pearls based on optical coherence tomography images," Sci. Rep. **6**(1), 33819 (2016).
16. A. Zhang, Q. Zhang, C. L. Chen, and R. K. Wang, "Methods and algorithms for optical coherence tomography-based angiography: a review and comparison," J. Biomed. Opt. **20**(10), 100901 (2015).
17. F. E. Robles, C. Wilson, G. Grant, and A. Wax, "Molecular imaging true-colour spectroscopic optical coherence tomography," Nat. Photonics **5**(12), 744–747 (2011).
18. U. Morgner, W. Drexler, F. X. Kärtner, X. D. Li, C. Pitris, E. P. Ippen, and J. G. Fujimoto, "Spectroscopic optical coherence tomography," Opt. Lett. **25**(2), 111–113 (2000).
19. T. E. Matthews, M. Medina, J. R. Maher, H. Levinson, W. J. Brown, and A. Wax, "Deep tissue imaging using spectroscopic analysis of multiply scattered light," Optica **1**(2), 105–111 (2014).
20. R. N. Graf, F. E. Robles, X. Chen, and A. Wax, "Detecting precancerous lesions in the hamster cheek pouch using spectroscopic white-light optical coherence tomography to assess nuclear morphology via spectral oscillations," J. Biomed. Opt. **14**(6), 064030 (2009).
21. Y. Zhao, J. R. Maher, J. Kim, M. A. Selim, H. Levinson, and A. Wax, "Evaluation of burn severity in vivo in a mouse model using spectroscopic optical coherence tomography," Biomed. Opt. Express **6**(9), 3339–3345 (2015).
22. H. S. Nam and H. Yoo, "Spectroscopic optical coherence tomography: A review of concepts and biomedical applications," Appl. Spectrosc. Rev. **1324876**, 1–21 (2017).
23. W.-H. Su, H.-J. He, and D.-W. Sun, "Non-Destructive and rapid evaluation of staple foods quality by using spectroscopic techniques: a review," Crit. Rev. Food Sci. Nutr. **57**(5), 1039–1051 (2017).
24. K. A. Vermeer, J. Mo, J. J. A. Weda, H. G. Lemij, and J. F. de Boer, "Depth-resolved model-based reconstruction of attenuation coefficients in optical coherence tomography," Biomed. Opt. Express **5**(1), 322–337 (2014).
25. Y. Sun and M. Lei, "Automated thickness measurements of nacre from optical coherence tomography using polar transform and probability density projection," in Proceedings of 2010 International Symposium on Intelligent Signal Processing and Communication Systems (ISPACS),(IEEE, 2010), pp1–4.
26. M. Lei, Y. Sun, D. Wang, and P. Li, "Automated thickness measurements of pearl from optical coherence tomography images." in Proceedings of Ninth International Conference on Hybrid Intelligent Systems, (IEEE, 2009), pp 247–251 (2008).
27. F. Robles, R. N. Graf, and A. Wax, "Dual window method for processing spectroscopic optical coherence tomography signals with simultaneously high spectral and temporal resolution," Opt. Express **17**(8), 6799–6812 (2009).

1. Introduction

Chinese freshwater pearls (CFWP), the most popular organic gems, are cultured in different kinds of living, mother oysters and mussels [1]. The growing market for CFWP has led to an increase in artificial pearl production. However, the lack of information about authentic pearl culturing limits efficient differentiation of authentic from artificial pearls [2-3]. Thus, finding an effective tool for pearl discrimination is necessary.

Pearl grading is a key component of evaluation, with various techniques under evaluation. Raman spectroscopy offers some discrimination [4] with spectral differences seen [5]. Raman vibrational bands reveal that natural pearl is comprised of biogenic calcium carbonate (nacre) while artificial pearls contain materials such as glass and plastic. Gemological microscopes are also useful, revealing whether the pearl surface is imitation or color treated. Using ultraviolet lamps, luminescence from pearls can reveal surface color treating [6]. Moreover, diffuse reflectance UV-Vis-NIR spectroscopy can reveal pigment characteristics, and thus discriminate between natural and artificial coloring [7].

Although the above methods are readily applied in pearl quality assessment, they do not fulfill the demands of reliably discriminating authentic and artificial pearls. Optical or luminescence microscopes distinguish pearls by surface texture under magnification, but in the Chinese pearl industry, freshwater pearls are almost always polished in order to get a desired shape and thus visual inspection is not reliable [8]. Surface reflectance only probes superficial regions of the pearl. However, some artificial pearls are covered with an 'imitation' layer that can be classified as authentic using surface examination, preventing accurate discrimination.

X-ray imaging is widely employed in the industry for observing the internal structure of pearls [9-10]. While X-ray techniques are effective at measuring the thickness of a nacre layer [11], they are not as useful for authenticity because the contrast does not distinguish material

Optical Materials EXPRESS

type. Further, previous results [12] show the luster of X-ray subjected pearls was reduced after extended exposure. Thus, a reliable industrial standard for fast, non-destructive discrimination of authentic and artificial pearls is still needed.

Optical Coherence Tomography (OCT), has advantages for pearl characterization, including high resolution and non-destructive testing [13]. Because nacre is highly scattering, the internal structure generates high contrast in OCT, making it easy to detect internal defects, and to measure the thickness of the nacre layer, key factors in pearl quality [14]. Combined with laser-induced fluorescence (LIF), pearl treatments such as bleaching, buffing, coating, filling and dyeing are reveals [12]. The species of mother oyster can also be discerned via fluorescence lifetime. Yang et al have also located internal defects within CFWP via OCT images through a fully automated algorithm based on graph segmentation [15]. Previous work has also reported using OCT in CFWP quality evaluation, and suggests that it can be used as a potential tool for fast and non-destructive diagnosis of the internal structure of pearls.

In order to classify pearls, OCT image features such as grayscale, texture, shape and spatial relationship are used [16]. However, this approach has not been effective for authentic and artificial CFWP discrimination. While OCT provides pixel intensity at micron scale resolution, distinguishing between authentic and artificial pearls requires material/molecular level information. Similar to X-ray examination, discerning material composition using grayscale differences from OCT images is not reliable, however, combining OCT with spectroscopic contrast has potential to provide the needed molecular information [17].

In this study, we propose a new approach based on acquiring depth-resolved NIR spectra using S-OCT [18]. This technique assesses spectroscopic features at different internal positions, as a function of wavelength [19]. S-OCT has been used in biological imaging such as early cancer detection of *in vivo* tissues [20]. Recently, we have used S-OCT to objectively evaluate burn injuries of *in vivo* mouse tissue, finding that spectral differences were highly correlated with the depth of the injury from histopathological images [21]. Using this same experimental scheme, we acquired spectroscopic data from the interior of pearls non-destructively. Below, we present a spectral analysis approach, based on principal component analysis (PCA) and partial least-squares discriminate analysis (PLSDA) models, that permits discrimination of authentic versus artificial pearls.

2. Material and methods

We used an experimental OCT system (SPARC DC) from Wasatch Photonics Inc, Durham, NC, with the central wavelength of 850 nm and 3dB bandwidth of 155 nm. The axial resolution, lateral resolution and imaging range in air were 2 μm, 10 μm and 1.9 mm, respectively. The maximum power delivered to the sample was 750 μW. The system includes a MEMS mirror scanning probe and 2048 pixel spectrometer. A-scan images were acquired by the included Spark OCT software while the spectroscopic and image processing was carried out via custom code with a GUI written in MATLAB (V2015, Mathworks, USA).

Authentic Chinese freshwater pearls were provided by Ruanshi Pearls Inc. (Shaoxin City, China), one of the leading enterprises in the industry. Twenty pearl samples were selected at random, including multiple color variants. The authentic pearls were cultured in *Hyriopsis cumingii,* the most commonly used 'mussel', and screened based on visual criteria to make sure that every CFWP pearl was authentic. Twenty artificial pearls were purchased, including 6 plastic (ABS), 7 glass (GLA) and 7 mother of pearl (MOP). Figure 1 shows photographs of both authentic and artificial pearl samples. Without any additional preparation, all samples were directly scanned by the OCT system, with a field of view of 1024x1024 pixels. The depth-resolved spectroscopic data were acquired from raw interferometric signals using custom software. In OCT images, low intensity signals can be dominated by speckle noise, producing inaccurate spectral data when processed. In order to reduce this noise in the OCT images, a grayscale threshold was established where OCT signals attenuated by a factor of e^{-1} compared to the level at the surface were excluded from spectroscopic processing. All

Optical Materials EXPRESS

interferometric signals were processed with a short time Fourier transform (STFT) using a spectral window of 122 cm^{-1} producing approximately 5 nm spectral resolution, and a coincident reduction of axial resolution from 2 to 63 μm [22]. Based on the homogeneity of internal composition, the authentic and artificial pearls were classified using spectrum averages from each OCT image. In the classification procedure, both supervised and unsupervised discrimination methods, including PCA and PLSDA, were employed [23]. Before imaging the pearl samples, a reference standard (Spectralon) was used to calibrate the spectral profiles at various depths.

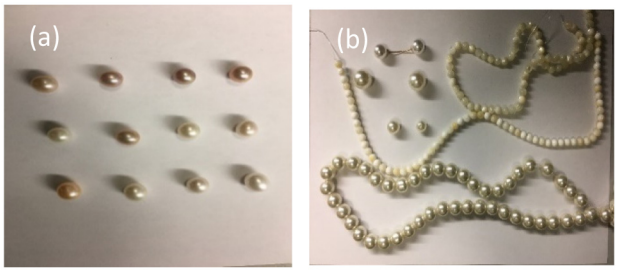

Fig. 1. Photographs of pearl samples; (a) Authentic CFWP; (b) Artificial pearls.

3. Results

Typical OCT images of CFWP, ABS, GLA and MOP are shown in Fig. 2 where yellow pixels were above the threshold of the nacre layer. It was found that light penetration in the CFWP was deeper than in ABS, GLA, and MOP since the annual ring structure of nacre in authentic pearls is more homogenous than artificial materials. For the GLA group, the penetration depth of light was less than in ABS because glass does not reflect enough light to provide a strong OCT signal. MOP samples have an inhomogeneous structure that will return reflected light depending upon the location of the OCT objective focus. Overall, Fig. 2(a)-(d) shows that there is little light penetration difference between the several sample groups, making it difficult to distinguish authentic and artificial pearls based on OCT intensity alone. Figure 2(a)-2(d) (insets) also show average logarithmic depth-intensity profiles for each selected pearl sample. The small yellow squares indicate penetration depth, defined as the location where the OCT signal was attenuated by a factor of e^{-1}. The intensity at this depth was used as a threshold for the grayscale images. By fitting a line to the logarithm of OCT depth profile (from signal peak to penetration depth) as shown in [24], the attenuation coefficient was determined. Figure 2(e) plots the attenuation coefficients of all the pearl samples from this study. Visual inspection of this plot shows that this approach cannot be used to discriminate pearl types with high accuracy.

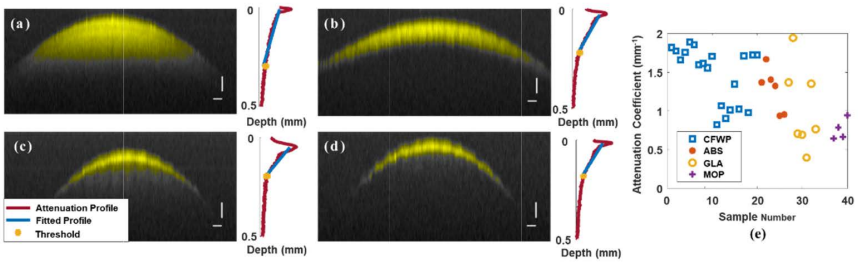

Fig. 2. Selected pearl samples; (a) CFWP; (b) ABS; (c) GLA; (d) MOP; The pixels colored yellow indicate that the intensity is greater than threshold. (Scalebars at lower right equal 250 um) ; Insets of (a)-(d): Average normalized logarithmic depth-intensity profiles; The yellow squares indicate depth were the OCT signal was attenuated by a factor of 1/e. (e) Attenuation coefficients of all the pearl samples.

Optical Materials EXPRESS

Significant spectral differences can be seen in the average spectra of four classes pearl after STFT processing (Fig. 3, left). Classification using Principal Components Analysis (PCA) was performed on the spectral data obtained via STFT. We monitored the percent variance captured by the PCA model, and set 20 PCs as maximum, which accounted for more than 99% of the cumulative variance. Figure 3 (Middle) shows the scores of first (PC1) and second (PC2) principal components and their basis spectra for each sample. This plot shows it is easy to distinguish authentic from artificial pearls. Moreover, it was possible to discriminate between certain artificial pearl groups, except for GLA and MOP, which had similar PC1 and PC2 scores. PCA scores could not avoid classification errors off these two types.

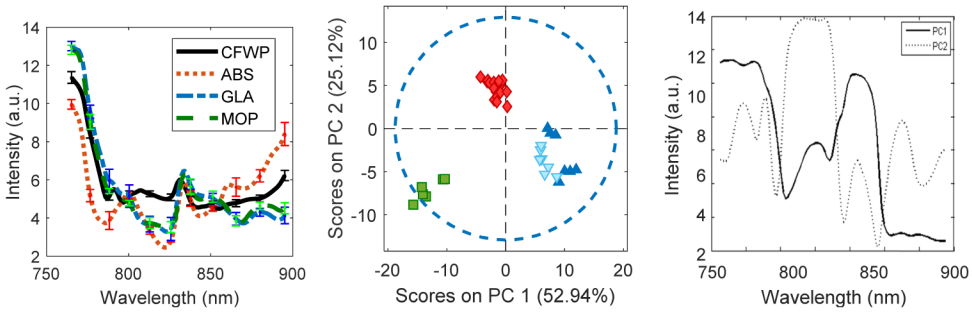

Fig. 3. (Left) Average spectra of four pearl classes. Error bars show intra-class standard deviation. (Center) Score Plot of first principal component (PC1) versus second principal component (PC2). (Right) Basis spectra for PC1, PC2.

For spectral analysis, an unsupervised PCA method was used to assess performance with one supervised method, PLS-DA, also evaluated for comparison. PLS-DA is the inverse-least-squares approach to LDA and produces essentially the same result but with the noise reduction and variable selection advantages of PLS. When applying the PLS-DA model, the average spectra were divided into the four groups described above. Leave one out cross validation was used to verify performance. In both models, 20 components were used, and variation in each sample was tested by Q^2 residuals and Hotellings T^2 tests to avoid outliers. Receiver operating characteristic (ROC) curves were used in the PLS-DA model to obtain an optimal threshold for classification. Table 1 shows prediction results of the PLS-DA model, which are nearly identical to PCA, proving that the PLS-DA model was able to classify CFWP and ABS groups. However, the GLA and MOP groups were not well separated due to the material similarity.

Table 1. PLS-DA results for classification of four groups of pearls

Indicator	CFWP	ABS	GLA	MOP
Sensitivity (CV)	1.00	1.00	0.857	0.857
Specificity (CV)	1.00	1.00	0.939	0.939
Class. Err (CV)	0%	0%	10.17%	10.17%

Table 2. PLS-DA results for classification of two groups of pearls

Indicator	CFWP	ABS/GLA/MOP
Sensitivity (CV)	1.00	1.00
Specificity (CV)	1.00	1.00
Class. Err (CV)	0%	0%

Nevertheless, the objective of this research was to distinguish authentic pearls from artificial ones. With this goal in mind, we repeated the analysis with the pearl samples divided only into two groups (CFWP and ABS/GLA/MOP). Table 2 shows two group prediction

Optical Materials EXPRESS

results of the PLS-DA model, providing ideal sensitivity, specificity and classification error of 1.00, 1.00 and 0% respectively.

4. Discussion

The use of S-OCT has been examined for determining the authenticity of pearls. Based on the utility of other spectroscopic methods, such as Raman and infrared spectroscopy, the added depth resolution of S-OCT was expected to improve discrimination. Natural Chinese freshwater pearls have a layered structure, composed of nacre formed by a mixture of calcium carbonate and organic binding agents. Nacre is semi-translucent, and most of the light striking the surface is reflected by different layers, creating the iridescent and luster characteristics for which pearls are known. However, this aspect also limits the reliability of spectroscopic based methods which focus just on the surface layer. A fake surface coating such as an iridescent varnish can fool these methods. On the other hand, the depth resolution of S-OCT can provide objective classification. We have also developed the dual window (DW) method for processing S-OCT signals to simultaneously achieve high spectral and axial resolution [27]. In cases where spectral features are not uniform across the sample, the (DW) method can be used.

Recently, nacre thickness, internal structure analysis, species and treatment classification by OCT have been reported [12,14,25,26]. Based on those applications, the morphological analyses of pearls made by OCT has been an important tool to discover the treatments made on pearls. Unfortunately, without the help of time-integrated fluorescence spectra, analysis by OCT images alone was unable to reveal the pearl origin, which prompted us to use S-OCT for authentic and fake CFWP classification.

Overall, S-OCT technique has several advantages compared with traditional methods, such as high resolution, acquisition speed, and noninvasive, nondestructive measurement, with applicability to all types of pearls. S-OCT allows the classification of authentic and fake CFWP, however OCT without spectroscopy presents some limitations mainly because it is an intensity based image analysis. Extending to S-OCT shows greater capability for appraising and identifying pearls. OCT images clearly delineated the internal structure of a pearl, and the spectrum generated by the images helped in evaluating and identifying pearls.

5. Conclusion

In this study, SOCT was used to analyze and classify authentic and fake pearls using both PCA and PLS-DA models. The depth resolved spectroscopy method proposed here shows excellent classification performance with 100% classification accuracy. A strong correlation was seen between internal spectroscopy and pearl material suggesting that this approach could be effective for discriminating authentic and fake Chinese freshwater pearls.

However, it is still difficult to distinguish the specific materials of fake pearls using our current SOCT approach. The main drawback of this S-OCT scheme for pearl classification was the bandwidth limitation, where S-OCT only provides a few hundred nanometers of spectral information as set by the light source in the OCT system. Although this was sufficient to make authentic and fake pearl discrimination, it was unable to make precise material classification for the fake pearls. An S-OCT system with broader bandwidth can likely obtain enough information for material discrimination. In authentic industrial applications, the classification and internal check of pearls need to penetrate the full depth extent, however, our results suggest that spectral analysis of just the outer part of the pearl was adequate. However, further development of new spectroscopic techniques with improved penetration depth and greater spectral coverage could potentially be used to monitor structural properties of whole pearls.

Optical Materials EXPRESS

Funding

National Science Foundation (NSF) (CBET 1604562); National Institute of Health (R01 CA210544).

Acknowledgments

This work was supported by the NSF CBET 1604562. Y. Z. was supported by a grant from the China Scholarship Council, No. 201608330413. We also thank the National Institute of Health (R01 CA210544), Dr. Silvia Ceballos and Jason Patrick for editing manuscript, Prof. Xi Feng and Yang Shi for collecting pearl samples.